Electrochemical and Solid-State Letters, **5** (6) A111-A114 (2002)
0013-4651/2002/5(6)/A111/4/$7.00 © The Electrochemical Society, Inc.

The Character of Dislocations in $LiCoO_2$

H. Gabrisch,[a,*,z] R. Yazami,[b] and B. Fultz[a,*]

[a]*Division of Engineering and Applied Science, California Institute of Technology, Pasadena, California 91125, USA*
[b]*Laboratoire d'Electrochimie et de Physicochimie des Matériaux et des Interface, Institut National Polytechnique de Grenoble/CNRS (UMR 5631), 38402 St. Martin d'Hères, France*

Dislocations in $LiCoO_2$ were observed by transmission electron microscopy, and their Burgers vectors were determined by analysis of diffraction contrast in tilting experiments. The configuration of all dislocations indicates that they are glissile, and dislocation configurations were found that are indicative of active slip planes. Perfect dislocations of $a/3\langle 11\bar{2}0\rangle$ type Burgers vectors were observed on {0001} habit planes. These perfect dislocations sometimes dissociate into Shockley partial dislocations with $a/3\langle 10\bar{1}0\rangle$ type Burgers vectors. Glide of these partial dislocations can account for the sequence of crystal structures O3, H1-3, O1 that occur with the delithiation of $LiCoO_2$. The presence of glissile dislocations also suggests possible damage mechanisms during cycling.
 [DOI: 10.1149/1.1472257]

Manuscript submitted November 9, 2001; revised manuscript received December 20, 2001. Available electronically April 2, 2002.

$LiCoO_2$ is the most commonly used material for positive electrodes (cathodes) in rechargeable Li-ion batteries. It has a high operating voltage *vs.* a lithium electrode (3.5-4.2 V), and a large specific capacity (approximately 140 mAh/g).[1] During charge and discharge cycles, lithium ions are extracted from and reintercalated into the $LiCoO_2$ crystals, a process during which nonstoichiometric $Li_{1-x}CoO_2$ compounds are formed. The specific capacity is limited by the stability of the crystal structure with extraction and intercalation of Li ions. X-ray diffractometry has shown that the lattice is preserved when the lithium content is cycled between $x = 0$ and $x \approx 0.5$. At a lithium content $(1 - x)$ of 0.5-0.45, however, the lithium ions in the O-Co-O framework undergo an order-disorder transition that is coupled to a change in the crystal lattice.[2-4]

Stoichiometric $LiCoO_2$ in its layered structure has a trigonal crystal lattice with $R\bar{3}m$ symmetry (space group 166), denoted the O3 structure. The unit cell can be indexed as rhombohedral or hexagonal. We choose hexagonal coordinates to illustrate the layered character of the material. In Fig. 1 a schematic of the hexagonal unit cell is shown. Oxygen atoms form a hexagonal lattice in CBACBA stacking with alternating layers of Li and Co atoms occupying the octahedral sites between them ($a = 2.82$ Å, $c = 14.06$ Å). The strong ionicity of the Co-O bonds leads to an important negative charge on the oxygen anions that destabilizes the layered structure. The cohesiveness of the system is maintained by insertion of cations (Li^+) between the O-Co-O slabs,[5] which are stacked as ABCABC.

The O-Co-O framework of the O3 structure of stoichiometric $Li_1Co_1O_2$ can be transformed to H1-3 and O1 structures by stacking of the O-Co-O slabs. Complete extraction of Li from the lattice results in the formation of a single-layered hexagonal phase CoO_2, denoted O1. Upon reinsertion of Li, this O1 structure converts back to the three-layered, delithiated O3 $Li_{1-x}CoO_2$ phase.[6] However, O1 CoO_2 is believed to be metastable;[7] therefore the stoichiometric change should be limited to $\Delta x \approx 0.5$ to achieve an acceptable cycle life (more than approximately 500 cycles).

Our knowledge of the crystallographic structures of $Li_{1-x}CoO_2$ has been obtained from X-ray and neutron diffractometries. Here we report a transmission electron microscopy (TEM) analysis of the dislocation structure in $LiCoO_2$. The samples were virgin material not yet subjected to the charging process (first Li deintercalation). The study of dislocations in this material is of interest for several reasons. Dislocations may provide an energetically favored diffusion path for the transport of Li ions between the electrolyte/electrode interface and their lattice site in the crystal structure.[8,9] The dislocations are also potential initiation sites for mechanical degradation of the material during charge/discharge cycling. Dislocations in $LiCoO_2$ have been reported previously[10] but have not been characterized. The present results show that perfect dislocations of $a/3\langle 11\bar{2}0\rangle$ type Burgers vectors are present in the material. These dislocations are in configurations that would enable glide, and evidence of glissile dislocations on a slip plane is reported. We also report that some of the perfect dislocations dissociate into Shockley partial dislocations. These partial dislocations could provide the translations of O-Co-O slabs that are needed for a mechanism of the O3-H1-3-O1 structural transformations.

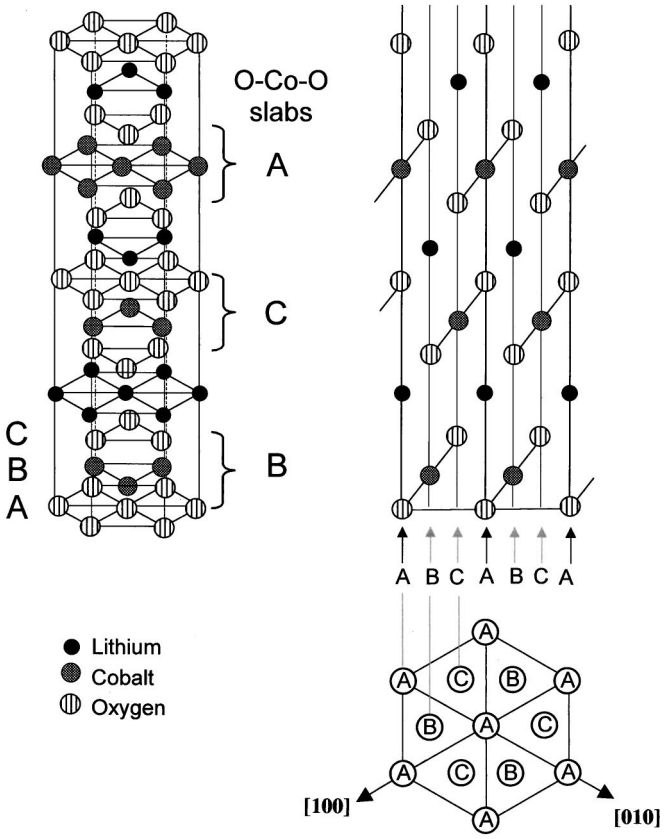

Figure 1. The layered structure of $LiCoO_2$ with $R\bar{3}m$ symmetry.

* Electrochemical Society Active Member.
z E-mail: heike@hyperfine.caltech.edu

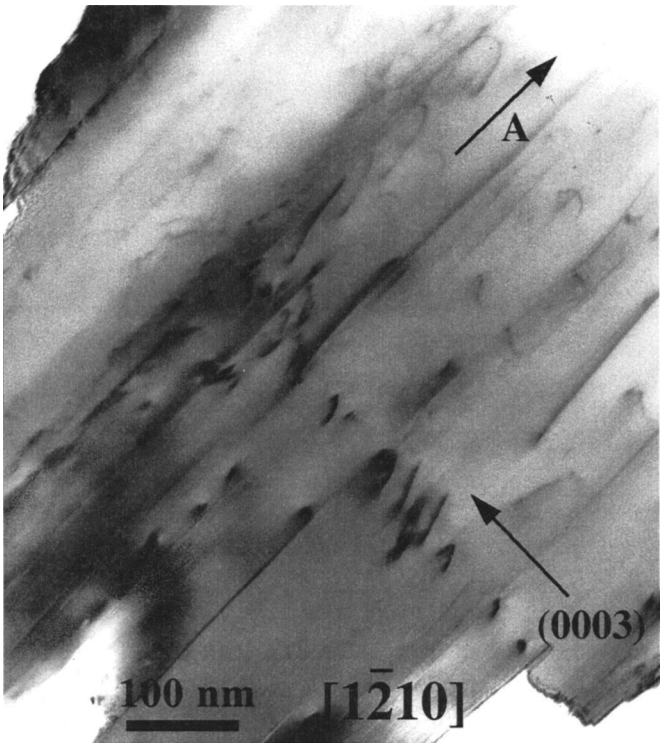

Figure 2. Arrays of dislocations in planes steeply inclined to the beam. To the left of arrow A, dislocations are seen bowing out in their glide plane. The zone axis, $\mathbf{k}_o = [1\bar{2}10]$, bright-field image.

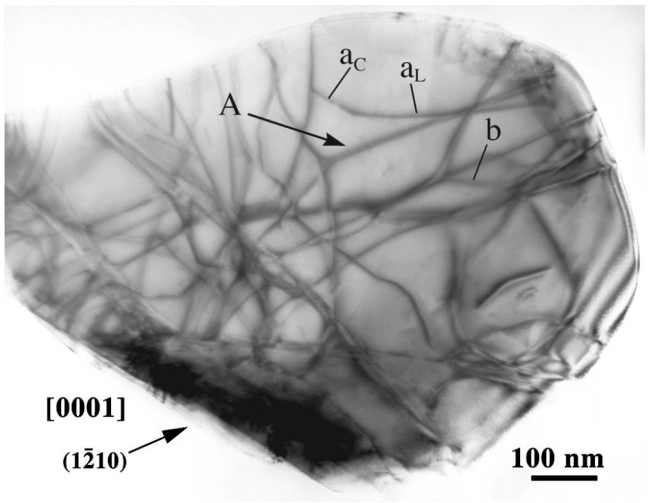

Figure 3. Dislocations lying in the basal plane, which is the zone axis ($\mathbf{k}_o$) of the image. Perfect dislocations with Burgers vectors of $a/3\langle 11\bar{2}0\rangle$ type have interacted and formed a network of perfect and partial dislocations. The dissociation of a perfect dislocation into Shockley partial dislocations according to the reaction $a/3[1\bar{2}10] \rightarrow a/3[1\bar{1}00] + a/3[0\bar{1}10]$ is indicated by arrow A.

Methods and Materials

Samples of $LiCoO_2$ were provided by the courtesy of ENAX Inc. (Japan). The TEM specimens were prepared by dusting $LiCoO_2$ powder onto a holey carbon film on a copper grid. A Philips EM420 transmission electron microscope operated at 120 kV was used for all investigations.

For Burgers vector analyses of the dislocations, each particle was imaged in several two-beam bright-field conditions. Additionally the particle was projected from several low-index zone axes to determine the line direction. The Burgers vector of a dislocation can be determined from the two-beam conditions in which the dislocation becomes invisible. In isotropic solids, the general condition for invisibility of a perfect dislocation is $\mathbf{g} \cdot \mathbf{b} = 0$, where $\mathbf{b}$ is the Burgers vector and $\mathbf{g}$ is the reciprocal lattice vector normal to the diffracting plane. Partial dislocations may be invisible for $\mathbf{g} \cdot \mathbf{b}_p = 0$ or $\pm 1/3$.[11] The line directions of the dislocations were obtained from projections of the dislocation in three or four different zone axes. In each projection, the dislocation lies in the plane that includes both the projected line direction and the direction of the electron-beam (zone axis). The intersection of at least two such planes gives the true line direction in space. It also contains the zone axes of both planes. On a stereographic projection, the projected line direction of the dislocation for each zone axis is marked on the great circle of that zone axis. The dislocation line direction is the pole of the great circle drawn through these points.[12]

Results

Figure 2 shows arrays of dislocations moving in glide planes that are steeply inclined with respect to the beam. (The dislocation segments terminate at the top and bottom surfaces of the sample.) A typical in-plane view of a dislocation substructure, seen along the [0001] zone axis, is shown in Fig. 3. Detailed analyses of the Burgers vectors of the dislocations revealed that slip takes place along $\langle 11\bar{2}0\rangle$ lattice directions in {0001} planes. From the analysis of the line directions $\mathbf{s}$, we found dislocations in near screw orientation, with the angle α between Burgers vector and line direction being 10-20° (perfect screw dislocation $\alpha = 0°$). An example is the dislocation segment marked a_L in Fig. 3, with Burgers vector $a/3[1\bar{2}10]$, line direction $\mathbf{s} = [1\bar{3}20]$, and angle $\alpha = 10°$. Where the dislocation character reveals a distinct edge component (α = 30-50°), the glide plane can be determined. Examples are the dislocation segment a_C and dislocation segment b in Fig. 3. Both dislocations have Burgers vectors $a/3[1\bar{2}10]$ and the following line directions: $\mathbf{s} = [\bar{1}2\bar{3}0]$, $\alpha = 50°$ for the segment a_C, and line direction $\mathbf{s} = [0\bar{1}10]$, $\alpha = 30°$ for dislocation segment b. The glide plane is the basal plane {0001}.

Some of the perfect dislocations in Fig. 3 have dissociated, forming Shockley partial dislocations in the reaction

$$a/3\langle 11\bar{2}0\rangle \rightarrow a/3\langle 10\bar{1}0\rangle + a/3\langle 01\bar{1}0\rangle \qquad [1]$$

One pair of Shockley partial dislocations is marked by arrow A in Fig. 3. The partial dislocations have Burgers vectors $a/3[1\bar{1}00]$ and $a/3[0\bar{1}10]$, and they have formed from dissociation of a perfect dislocation with a Burgers vector $a/3[1\bar{2}10]$.

In Fig. 4 the same Shockley partial dislocations are imaged under different diffraction conditions. Table I presents the visibility criteria for the perfect dislocation ($\mathbf{b} = a/3[1\bar{2}10]$) and the two partial dislocations ($\mathbf{b} = a/3[1\bar{1}00]$ and $\mathbf{b} = a/3[0\bar{1}10]$) for the diffraction conditions used in the analysis. In Fig. 4a both dislocation lines are visible when imaged with $\mathbf{k}_0 = [\bar{2}021]$ and $\mathbf{g} = (1\bar{2}10)$. In Fig. 4b only the partial dislocation with Burgers vector $a/3[1\bar{1}00]$ is visible viewed from the same zone axis as Fig. 4a, $\mathbf{k}_o = [\bar{2}021]$, but with a different lattice diffraction $\mathbf{g} = (11\bar{2}6)$. In Fig. 4c both dislocation lines are extinct under the diffraction condition $\mathbf{k}_o = [10\bar{1}1]$ and $\mathbf{g} = (10\bar{1}\bar{2})$. The comparison between Fig. 4a where both dislocation lines are visible and Fig. 4b where only the partial dislocation with $\mathbf{b} = a/3[1\bar{1}00]$ is visible, clearly demonstrates that the observed configuration is not a dislocation dipole. Dislocation dipoles have the same invisibility criteria for both dislocation lines. The two partial dislocations are separated by approximately 5 nm.

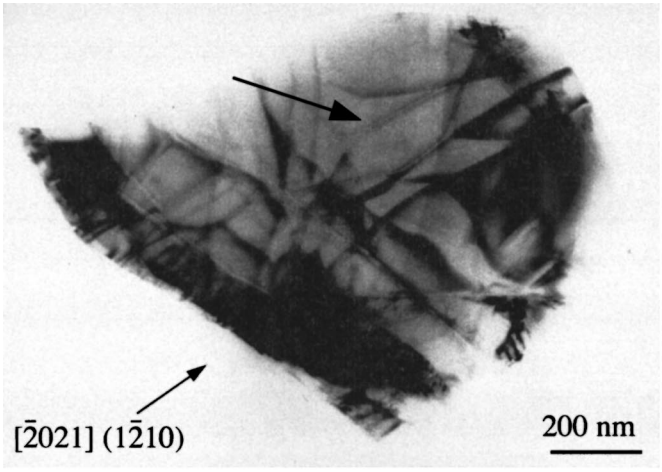

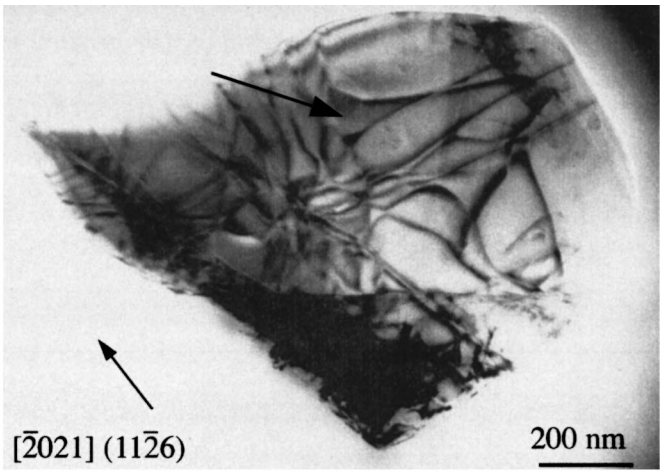

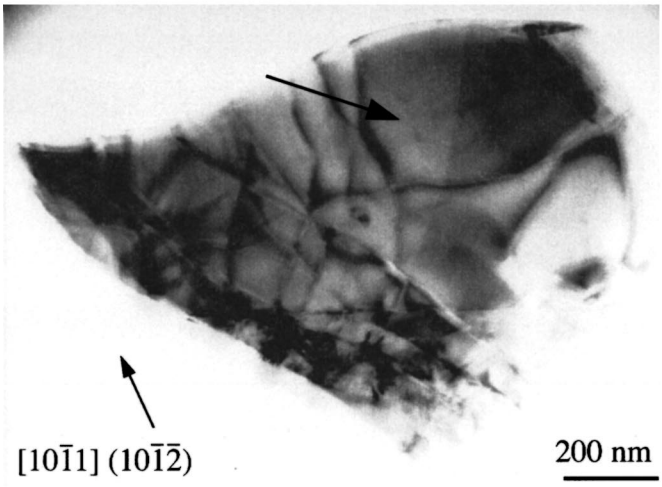

Figure 4. Partial dislocations formed from the reaction $a/3[1\bar{2}10] \rightarrow a/3[1\bar{1}10] + a/3[0\bar{1}10]$ imaged under different diffraction conditions. (a, top left) $\mathbf{k}_o = [\bar{2}021]$ with active diffraction $\mathbf{g} = (1\bar{2}10)$ shows both dislocation lines as visible. (b, above) $\mathbf{k}_o = [\bar{2}021]$ $\mathbf{g} = (11\bar{2}6)$ shows partial dislocation with Burgers vector $a/3[0\bar{1}10]$ as visible, while partial dislocation with $\mathbf{b} = a/3[1\bar{1}00]$ is invisible. (c, left) $\mathbf{k}_o = [10\bar{1}1]$ $\mathbf{g} = (10\bar{1}\bar{2})$ shows both partial dislocations as invisible. The dislocations' line direction of the dislocation is [1210], and both partial dislocations have 30° character.

Table I. Invisibility criteria for the perfect dislocation with Burgers vector $a/3[1\bar{2}10]$ and the two partial dislocations formed by the reaction $a/3[1\bar{2}10] \rightarrow a/3[1\bar{1}10] + a/3[0\bar{1}10]$.[a]

g	**b** = $a/3[1\bar{2}10]$	**b**= $a/3[1\bar{1}00]$	**b**= $a/3[0\bar{1}10]$	$\mathbf{k}_o$
$(10\bar{1}\bar{2})$	x	x	x	$[10\bar{1}1]$, $[02\bar{2}1]$
$(\bar{1}011)$	x	x	x	$[\bar{1}101]$, $[0\bar{1}11]$
$(\bar{1}\bar{2}10)$	v	v	v	$[10\bar{1}1]$, $[\bar{2}021]$, $[0001]$
$(\bar{1}101)$	v	x	v	$[10\bar{1}1]$
$(1\bar{1}02)$	v	x	v	$[\bar{1}101]$
$(\bar{2}204)$	v	v	v	$[\bar{3}122]$
$(\bar{2}110)$				$[0\bar{1}11]$, $[02\bar{2}1]$, $[0001]$
$(01\bar{1}\bar{1})$	v	v	x	$[10\bar{1}1]$, $[\bar{1}101]$
$(01\bar{1}4)$	v	v	x	$[02\bar{2}1]$
$(11\bar{2}0)$	v	v	x	$[\bar{1}101]$
$(11\bar{2}6)$	v	v	x	$[\bar{2}021]$

[a] Visibility (v) and invisibility (x) conditions are given for the **g** vectors used in the experiments. The right column lists the directions of the incident beam ($\mathbf{k}_0$) that were used.

The stacking fault between the partial dislocations is ''intrinsic.'' An intrinsic fault changes the ABC-ABC stacking to ABC-BCA on a local scale.

Discussion

The dissociation of perfect dislocations into Shockley partial dislocations suggests mechanisms for structural transformations in the material. The dissociation of a perfect dislocation with $\mathbf{b} = a/3\langle 11\bar{2}0\rangle$ into partial dislocations with $\mathbf{b} = a/3\langle 10\bar{1}0\rangle$ and $\mathbf{b} = a/3\langle 01\bar{1}0\rangle$ changes the atom positions between the partial dislocations on successive layers from A to B to C. In Fig. 5 it is shown how the dissociation of a perfect dislocation into Shockley partial dislocations can change the stacking order of the Co-O-Co slabs. The strong bonding between the oxygen and cobalt layers in $LiCoO_2$ suggests that dislocation slip occurs only in the Li layers between the O-Co-O slabs. Figure 5a shows schematically the stackings in the *c* direction of the O-Co-O slabs of O3 $LiCoO_2$ (seen along the [110] direction, as indicated in Fig. 1). For simplification the Li layers are omitted and are indicated as gray lines. In Fig. 5b the stacking order of the O3 structure is shown after a partial dislocation has passed across every other Li layer (from right to left, as indicated by arrows). The stacking order in the oxygen lattice changes from C-B-A in the O3 structure to A-C-A-C-B-A-B-A-C-B-C-B of the H1-3 structure. Passage of the same Shockley partial dislocations across all Li layers changes the crystal to the C-B-C-B stacking of the O1 structure.

Figure 5 shows that all O-Co-O slabs have identical orientations in the O3, H1-3, and O1 structures. Glide of the observed partial dislocations reported here could be responsible for the transition

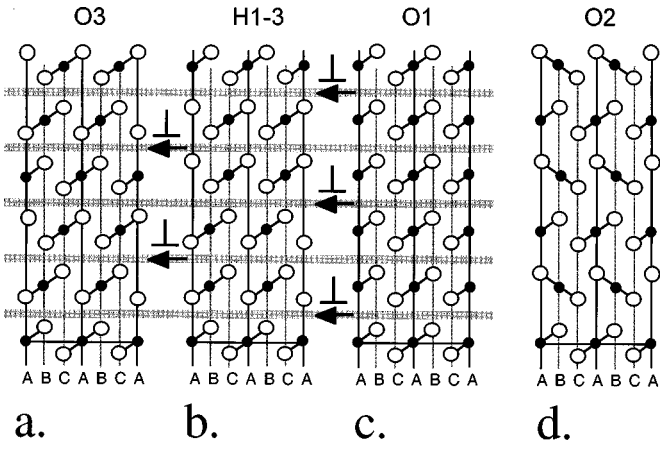

Figure 5. Transformation paths from O3 to H1-3 to O1 structures by passage of Shockley partial dislocations along the planes of Li atoms (shown in gray bands without Li atoms). Such dislocations having upper half-planes would pass from right to left to induce the required shears. The structure at right is the O2 structure, which cannot be obtained by passage of such dislocations along the Li planes.

between these structures. A transformation from the O3 to the O2 structure (shown in Fig. 5d) requires a change in orientation within the O-Co-O slabs. Perhaps it is useful to think that the O3-O2 transformation is suppressed by the high Peierls energy associated with dislocation movement between the Co and O atoms. Phase transformations by slip of Shockley partial dislocations have been reported before in silicon nitride for the transition from α to β phase.[13]

The 5 nm separation between the Shockley partial dislocations can be used to estimate the stacking fault energy. Assuming a shear modulus of 200 GPa, a stacking fault energy of approximately 50 mJ/m^2 is estimated from the expression[14]

$$\gamma = \frac{\mu}{2\pi r}\left[(\mathbf{b}_1 \cdot \boldsymbol{\zeta}_1)(\mathbf{b}_2 \cdot \boldsymbol{\zeta}_2) + \frac{(\mathbf{b}_1 \times \boldsymbol{\zeta}_1) \cdot (\mathbf{b}_2 \times \boldsymbol{\zeta}_2)}{1 - \nu}\right] \quad [2]$$

where γ is the stacking fault energy, μ is the Shear modulus, r is the spacing between the partial dislocations, $\mathbf{b}$ is the Burgers vector, $\boldsymbol{\zeta}$ is the dislocation line direction, and ν is the Poisson's ratio (here assumed $\nu = 0.3$). This estimate of γ is approximate because the shear modulus is uncertain, and the assumption of isotropic elasticity is probably invalid. Furthermore, the stacking fault energy is expected to change as lithium is removed from the material. If the partial dislocations are responsible for the phase transformations of the O3 structure, the separations between partial dislocations are expected to increase as the material is delithiated. (For comparison, the spacing between Shockley partials observed in AlN was observed to be 8 nm, and a stacking fault energy of 7.5 ± 1 mJ/m^2 was estimated using $\mu = 30$ GPa.[15])

The dislocations reported here are in a glissile configuration. Their motions could be part of a damage mechanism that proceeds with increased cycle life and that causes a reduction in the capacity of the battery. Changes in the defect structure with cycling may also alter the kinetics of Li diffusion in the material. Further studies of dislocations in cycled material and in material at partial states of delithiation are underway.

Conclusions

The perfect dislocations observed in virgin O3 $LiCoO_2$ material had $a/3\langle 11\bar{2}0\rangle$ Burgers vectors, and were of screw and mixed character. Where the perfect dislocations dissociated into Shockley partials according to the reaction $a/3[11\bar{2}0] \rightarrow a/3[10\bar{1}0] + a/3[01\bar{1}0]$, the glide plane could be determined to be the (0001) basal plane. The observed perfect and partial dislocations are in glissile configurations, and groups of dislocations have been observed that appear to have undergone some glide. Glide of partial dislocations on successive lattice planes could provide the mechanism for the transformations from the O3 to H1-3 to O1 structures that occur during delithiation.

Acknowledgments

The authors gratefully thank ENAX Inc. of Japan for the disposal of the sample material. This work has been supported by the U.S. Department of Energy through Basic Energy Sciences grant DE-FG03-00ER15035.

California Institute of Technology assisted in meeting the publication costs of this article.

References

1. J. B. Goodenough, in *Lithium Ion Batteries-Fundamentals and Performance*, M. Wakihara, O. Yamamoto, Editors, p. 1, Wiley-VCH, Weinheim (1998).
2. J. N. Reimers and J. R. Dahn, *J. Electrochem. Soc.*, **139**, 2091 (1992).
3. T. Ohzuku and A. Ueda, *J. Electrochem. Soc.*, **141**, 2972 (1994).
4. A. Van der Ven, M. K. Aydinol, and G. Ceder, *J. Electrochem. Soc.*, **145**, 2149 (1998).
5. C. Delmas, in *Lithium Batteries-New Materials, Developments and Perspectives*, G. Pistoia, Editor, p. 457, Elsevier, Amsterdam (1994).
6. G. G. Amatucci, J. M. Tarascon, and L. C. Klein, *J. Electrochem. Soc.*, **143**, 1114 (1996).
7. M. Broussely, P. Biensan, and B. Simon, *Electrochim. Acta*, **45**, 3 (1999).
8. J. H. Strange and S. M. Rageb, *Philos. Mag. A*, **64**, 1159 (1991).
9. I. Sakaguchi, Y. Yurimoto, and S. Sueno, *J. Am. Ceram. Soc.*, **75**, 712 (1992).
10. H. Wang, Y.-I. Jang, B. Huang, D. R. Sadoway, and Y.-M. Chiang, *J. Electrochem. Soc.*, **146**, 473 (1999).
11. P. G. Partridge, *Metall. Rev.*, **12**, 118, 169 (1967).
12. J. W. Edington, *Practical Electron Microscopy in Material Science*, p. 87, N.V. Philips Gloeilampenfabrieken, Eindhoven (1976).
13. X. Milhet, J. L. Demenet, and J. Rabier, *Eur. Phys. J.: Appl. Phys.*, **4**, 149 (1998).
14. J. P. Hirth and J. Lothe, *Theory of Dislocations*, 2nd ed., p. 315, Krieger Pub. Co. Malabar, FL (1982).
15. M. F. Delanot and J. Rabier, *J. Mater. Sci.*, **24**, 1594 (1989).